Universal critical behavior in single crystals and films of $YBa_2Cu_3O_{7-\delta}$

Hua Xu, Su Li, Steven M. Anlage, and C. J. Lobb*
Center for Nanophysics and Advanced Materials, Department of Physics, University of Maryland, College Park, Maryland 20742-4111, USA

M. C. Sullivan
Department of Physics, Ithaca College, Ithaca, New York 14850, USA

Kouji Segawa and Yoichi Ando
Institute of Scientific and Industrial Research, Osaka University, Ibaraki, Osaka 567-0047, Japan
(Received 21 July 2009; published 30 September 2009; corrected 6 October 2009)

We have studied the normal-to-superconducting phase transition in optimally doped $YBa_2Cu_3O_{7-\delta}$ in zero external magnetic field using a variety of different samples and techniques. Using dc transport measurements, we find that the dynamical critical exponent $z=1.54\pm0.14$, and the static critical exponent $\nu=0.66\pm0.10$ for both films (when finite-thickness effects are included in the data analysis) and single crystals (where finite-thickness effects are unimportant). We also measured thin films at different microwave frequencies and at different powers, which allowed us to systematically probe different length scales to avoid finite-thickness effects. dc transport measurements were also performed on the films used in the microwave experiments to provide a further consistency check. These microwave and dc measurements yielded a value of z consistent with the other results, $z=1.55\pm0.15$. The neglect of finite-thickness, finite-current, and finite-frequency effects may account for the wide ranges of values for ν and z previously reported in the literature.

DOI: 10.1103/PhysRevB.80.104518 PACS number(s): 74.40.+k, 74.25.Dw, 74.25.Fy, 74.72.Bk

I. INTRODUCTION

The high critical temperatures, large penetration depths, and short coherence lengths of high-temperature superconductors make it possible to measure critical fluctuations in these materials, in contrast to conventional superconductors.[1,2] In spite of nearly two decades of work, however, there is no experimental consensus on the critical exponents of the superconducting phase transition in zero magnetic field. By performing both dc and microwave measurements on thin films, and dc measurements on single crystals, and doing careful analysis of the data that properly accounts for finite size, current, and frequency effects, we are able to provide consistent values for the exponents.

There are two fundamental parameters which characterize a second-order phase transition such as the superconducting to normal transition.[1] The first is the temperature-dependent correlation length, $\xi(T)$, which is close to the transition temperature T_c varies as

$$\xi(T) \sim |T/T_c - 1|^{-\nu}, \tag{1}$$

where ν is the static critical exponent. A second parameter is the relaxation time $\tau(T)$, which close to T_c varies as

$$\tau \sim \xi^z \sim |T/T_c - 1|^{-z\nu}, \tag{2}$$

where z is the dynamic critical exponent.

It is generally accepted that, theoretically, $\nu \approx 0.67$ in a superconductor in zero magnetic field, since the phase transition belongs to the three-dimensional (3D) *XY* universality class.[3] The theoretical situation for the dynamical exponent z is less certain. Fisher *et al.*[1] argue that the number of Cooper pairs is not conserved, so that model *A* dynamics,[3] which give $z=2$, should apply. Other theoretical considerations yield $z=1.5$,[4] similar to model *E* dynamics. Lidmar[5] and Weber[6] present Monte Carlo simulations that suggest $z \approx 1.5$.

The exponent ν can be determined experimentally from a number of static experiments. In zero field, measurements of penetration depth,[7,8] magnetic susceptibility,[9–11] specific heat,[9,12] and thermal expansivity[13] largely agree that the static critical exponent $\nu \simeq 0.67$, and indicate that the phase transition in zero field belongs to the 3D-*XY* universality class. (Note, however, there are some measurements which yield different results.[9,14])

In principle dc conductivity measurements, which depend on both the statics and the dynamics of the order parameter near T_c, can determine both the static critical exponent ν and dynamical critical exponent z. The exponents ν and z are expected to be universal but values extracted from conductivity measurements are not consistent. For example, dc conductivity measurements yield a wide range of values for critical exponents: $\nu=0.63-1.2$ and $z=1.25-8.3$.[15–21]

ac measurements can determine both the real and imaginary parts of the fluctuation conductivity, providing another probe of critical dynamics.[1,18,22,23] Measurements over a broad frequency range allow one to probe the dynamical behavior of the system and directly measure the fluctuation lifetime.[18] These experiments are difficult and seldom done, and the available results are inconsistent, with values of z ranging from 2 to 5.6. Booth *et al.* investigated the frequency-dependent microwave conductivity of $YBa_2Cu_3O_{7-\delta}$(YBCO) films above T_c and obtained $z=2.3-3$.[18] Nakielski *et al.* measured the conductivity of YBCO at low frequency (<2 GHz) and obtained $z \approx 5.6$.[24] Osborn *et al.* did a similar experiment on $Bi_2Sr_2CaCu_2O_{8+\delta}$ and obtained $z \approx 2$.[25] For an optimally doped $La_{2-x}Sr_xCuO_4$(LSCO) film, Kitano *et al.* found that their data

 ©2009 The American Physical Society

were consistent with the 3D-*XY* model with diffusive dynamics, $\nu \approx 0.67$ and $z \approx 2$ in a certain temperature range.[26]

Although the critical exponents ν and z should be universal, we see that there is at present no consensus in the literature as to their values for the zero-field transition in the cuprate superconductors. In this paper we report the results of a variety of complimentary experiments which yield independent determinations of the critical exponents. In Sec. II, we discuss dc transport measurements on both thin films and thick single crystals. We present different ways to infer each exponent from measurements and show how finite-thickness effects in the films can confuse interpretation of the data in the limit of small currents. We also show that choice of the proper range of current can avoid the finite-thickness effects in films and show how application of a small magnetic field allows the determination of ν in both crystals and films.

In Sec. III, we discuss microwave measurements on thin films. Just as with dc measurements, microwave measurements require a nonzero current density. How the applied microwave current-density affects the measured response has not been systematically addressed. Recently Sullivan *et al.* argued that a finite-thickness effects at low-current density was the reason for previous inconsistent results in dc measurements.[19] The question of whether a finite-thickness effect influences the ac measurement and the extracted critical exponents, as in dc measurements, inspired us to study the power dependence of the microwave fluctuation conductivity. We find that several length scales play a role in ac conductivity measurements and only after their effects are properly accounted for can the underlying critical dynamics be understood. As a further check, after completing the microwave measurements, we repatterned the same samples and performed dc measurements.

When finite-size effects are properly accounted for, we find that *all* of our results are consistent. As discussed in detail below, we find ν is 0.66 ± 0.10 and z is 1.55 ± 0.15.

II. dc MEASUREMENTS ON SINGLE CRYSTALS AND FILMS

Our crystals are grown by a flux method using Y_2O_3 crucibles to ensure crystal purity.[27,28] The films are prepared by the pulsed-laser deposition technique at 850 °C and 150 mbar oxygen pressure on $SrTiO_3$ substrates.[29,30] Transport measurements were carried out using the standard four-probe method. The currents were applied along the *ab* plane for the films and along the *a* axis for the crystals. All connections to the sample are made through double T low-pass filters to reduce noise.[31] We measure the samples inside a cryostat covered with a μ-metal shield so that the residual magnetic field is less than 2×10^{-7} T. At 96 K, the resistivity of the crystal is around 70 $\mu\Omega$ cm and the resistivity of the film is around 90 $\mu\Omega$ cm.

In theory, log-log plots of electric field E vs current density J isotherms above T_c have positive curvatures and display nonlinearities in the high currents, as shown schematically in Fig. 1(a).

As T_c is approached from above, in the limit of $J \to 0$ (Ref. 1)

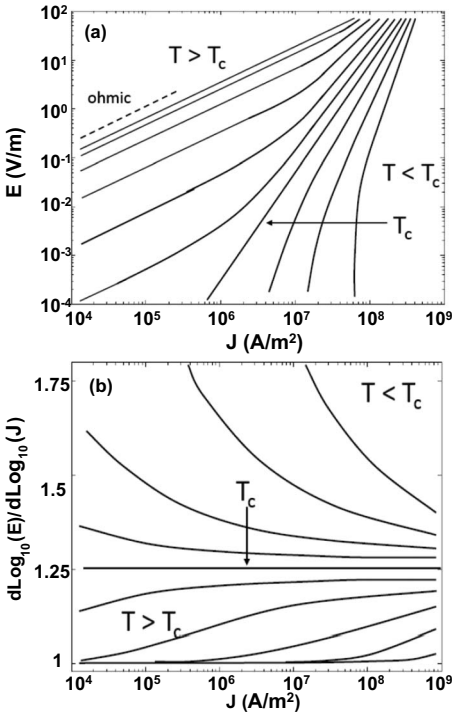

FIG. 1. Schematic plots of electric field E versus current density J. (a) E-J plot in log-log scale and (b) $d \log_{10}(E)/d \log_{10}(J)$ vs J in semilog scale.

$$\frac{E}{J} \sim \xi^{(D-2-z)}. \tag{3}$$

Thus, in a $\log(E)$ vs $\log(J)$ plot, isotherms above T_c exhibit ohmic behavior—a slope of one—at low currents. The isotherms below T_c have negative curvatures and display vanishing linear resistance ($R \to 0$ as $J \to 0$). At $T = T_c$, the critical isotherm is expected to show a power-law behavior[1]

$$E \sim J^{(z+1)/(D-1)} \tag{4}$$

which is a line with a slope greater than one on a $\log(E)$ vs $\log(J)$ plot.

In Fig. 2(a) we show selected E vs J curves in a log-log plot for an untwinned YBCO single crystal. From the figure, all isotherms above the dashed line (triangles) have positive curvatures and have ohmic response in the limit of zero current, and all isotherms below the dashed line (squares) have negative curvatures and display vanishing linear resistivity. We can verify this curvature by fitting the $E-J$ curves to a second-order form of $\log(E) = a_0 + a_1 \log(J) + a_2 [\log(J)]^2$, where we use the sign of a_2 to indicate the curvature of each isotherm. We find that a_2 is positive above 93.838 K and negative below 93.836 K.[32] Thus, from Fig. 2(a) we find $T_c = 93.837 \pm 0.003$ K. The dashed line in Fig. 2(a) separates the superconducting and normal states of the sample and the high-current part can be fit to $E \sim J^{1.22 \pm 0.10}$. From Eq. (4) (using $D = 3$), we find

$$z = 1.44 \pm 0.2. \tag{5}$$

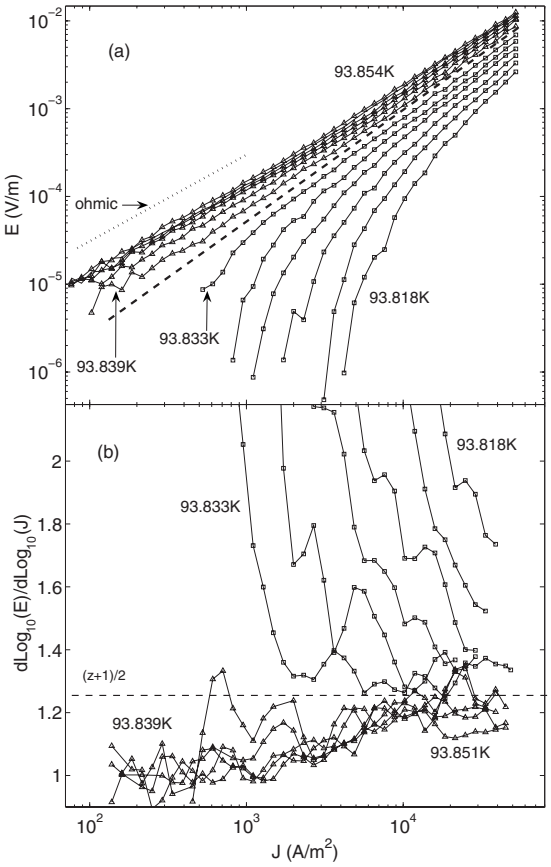

FIG. 2. (a) The electric field E versus current density J for an untwinned YBCO single crystal. The dashed line separates the normal and superconducting phases. The isotherms above the dashed line exhibits ohmic behavior at low-current density. The isotherms below the dashed line display the vanishing linear resistivity. Isotherms are separated by 3 mK. (b) Derivative plot of the data in Fig. 2(a). The dashed line separates the normal and superconducting phases. The crossing of the dashed line with isotherm of 93.839 K is due to the noise. Both plots indicate $z \approx 1.5$.

Another way to evaluate the power-law behavior is the $(\frac{\partial \log E}{\partial \log J})_T$ vs J plot.[29] From Eq. (4), at the transition temperature T_c

$$\left(\frac{\partial \log E}{\partial \log J}\right)_{T_c} = \frac{z+1}{D-1} \tag{6}$$

thus, the critical isotherm is a horizontal line parallel to the J axis in a derivative plot. The critical isotherm separates the monotonically increasing isotherms above T_c and the monotonically decreasing isotherms below T_c in the schematic Fig. 1(b). The derivative plot generally displays the phase transition more clearly than a basic plot of E vs J.

In Fig. 2(b), we show a derivative plot of the data shown in Fig. 2(a). The dashed line in Fig. 2(b) separates the normal and superconducting phases. The intercept of the dashed line is 1.25 ± 0.10 and is expected to be $(z+1)/2$ from Eq. (6). From the derivative plot, we find

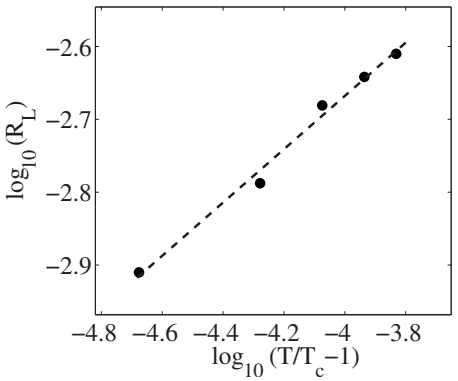

FIG. 3. Power law fit to Eq. (8) of the ohmic response of the isotherms just above the transition temperature T_c. Because $R_L \propto (T/T_c - 1)^{\nu(z-1)}$, we can use this line to find ν. By setting $T_c = 93.837 \pm 0.003$ K and $z = 1.5 \pm 0.20$, we get $\nu = 0.71 \pm 0.30$.

$$z = 1.50 \pm 0.20, \tag{7}$$

which is nearly identical to the result obtained from Fig. 2(a), using Eq. (4). Figure 2(b) also qualitatively shows the change in sign of a_2 discussed above.

The exponent ν can be found from the low-current ohmic behavior R_L above T_c by combining Eqs. (1) and (3) (Ref. 1)

$$R_L \propto (T/T_c - 1)^{\nu(z-1)}. \tag{8}$$

The slope of the $\log(R_L)$ vs $\log(T/T_c - 1)$ plot in Fig. 3, combined with Eq. (8), determines ν. We find

$$\nu = 0.71 \pm 0.30 \tag{9}$$

from Fig. 3.

We can apply a perpendicular magnetic field and look at the transition in finite field. According to Ref. 1, the difference between the critical temperature T_c and the melting temperature $T_{m(g)}(H)$ is

$$T_c - T_{m(g)}(H) \sim H^{1/2\nu}, \tag{10}$$

where ν is the zero-field static exponent. Equation (10) is expected to be true for clean crystals, where the transition is a first-order melting (m) transition, as well as for disordered films, where the transition is a glass (g) transition. We show $T_c - T_m(H)$ vs. $\mu_0 H$ in Fig. 4(a) and find

$$\nu = 0.68 \pm 0.10 \tag{11}$$

from a power-law fit. This result is consistent with the 3D-XY model and is also consistent with the result obtained from experiments using Eq. (8).

In Fig. 5(a), we show the $E-J$ curves for a 150-nm-thick YBCO c-axis-oriented optimally doped film. The isotherms differ by 0.05 K from 92.075 to 91.225 K. Unlike Fig. 2(a), we cannot find a single straight line in Fig. 5(a) that separates the isotherms into two groups which are either concave or convex exclusively. To help find the true critical isotherm, we again use the derivative plot,[29] where the critical isotherm ideally will correspond to a horizontal straight line, as in Figs. 1(b) and 2(b). However, in Fig. 5(b), there is no horizontal isotherm, and there are isotherms monotonically decreasing above 2×10^7 A/m^2, and also monotonically in-

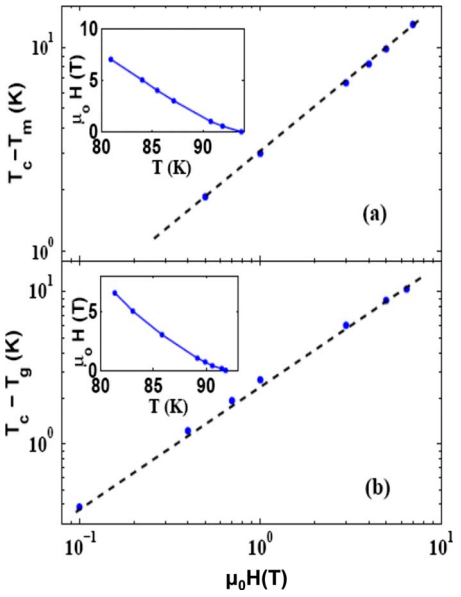

FIG. 4. (Color online) (a) $T_c - T_m$ vs $\mu_0 H$ of an untwinned YBCO single crystal. Here, as $T_c - T_m(H) \sim H^{1/2\nu}$, we can find ν from this line without assuming a value for z, and find $\nu = 0.68 \pm 0.10$. The inset is the melting line for the crystal up to 7 T. (b) A similar plot of $T_c - T_g$ vs $\mu_0 H$ for a YBCO thin film ($d \approx 150$ nm). From this curve we find $\nu = 0.63 \pm 0.10$. The inset is the glass transition line for the film up to 6.5 T.

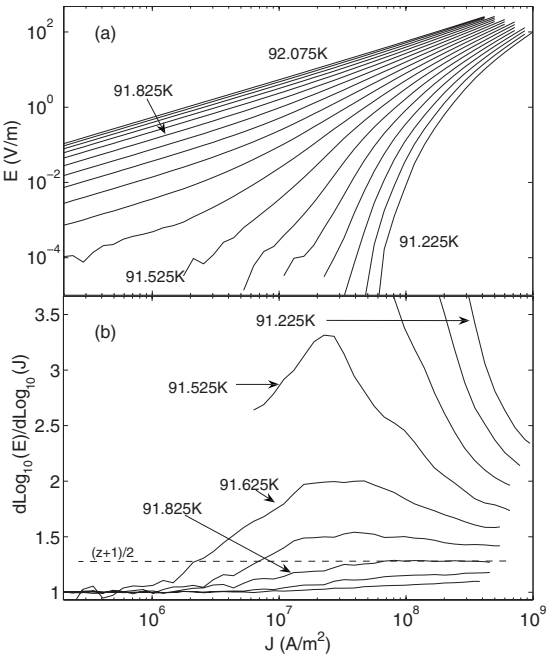

FIG. 5. (a) *E-J* isotherms for a 150 nm YBCO film in zero magnetic field. The spacing between isotherms is 50 mK. (b) The derivative plot of some selected isotherms from (a). At low-current-density regime, the phase transition is obscured by finite-size effects. The spacing between isotherms is 100 mK.

creasing below 2×10^7 A/m^2. So, if the experimental setup were to allow us to measure even smaller voltages, we would expect all of these isotherms would bend down toward 1 (ohmic behavior) in the derivative plot at smaller current densities.

The cause of this behavior is most likely finite-size effects.[19,33] Below the transition temperature, thermal fluctuations take the form of vortex loops.[34] As discussed in the Appendix, vortex loops with length scales of order

$$L_J \sim \sqrt{\frac{k_B T}{2\pi\Phi_0 J}} \tag{12}$$

are probed by current density J.[1,33] The loops with length scale smaller than L_J will shrink and cause no dissipation. At high-current density, such that L_J is less than the thickness of the sample d, the vortex loops probed in the experiment are still 3D like. However, at low-current density, such that $L_J > d$, the size of the vortex loops probed will be limited by the thickness of the sample and vortex antivortex pairs will be probed. This will lead to a nondiverging energy barrier causing ohmic behavior even below the bulk transition temperature. When L_J is equal to 150 nm, the thickness of the film used to produce the data in Fig. 5, the crossover current density is on the order of 5×10^6 A/m^2, which is close to where the isotherms bend towards ohmic behavior in Fig. 5(b).

Because of the finite-size effects, the conventional method picks an incorrect critical isotherm and exponent, contributing to the inconsistent results from previous transport experiments on high-T_c films. However, high-current data are not affected by finite-size effects, and we can extract the T_c and z from the high-current regime.[19] If we only look at the high-current regime in Fig. 5(b), it looks very similar to the schematic derivative plot [Fig. 1(b)] and the actual derivative plot of crystal data [Fig. 2(b)]. The dashed line in Fig. 5(b), which coincides in the high-current regime with the isotherm of 91.825 K, separates the two phases of the film. The transition temperature determined from the high-current regime is $T_c = 91.825 \pm 0.025$ K and the intercept of the dashed line is 1.27 ± 0.07. According to Eq. (6), from the high-current data

$$z = 1.54 \pm 0.14 \tag{13}$$

which agrees with the result from the crystal data. In addition, in our other *c*-axis-oriented YBCO films with the thickness d ranging from 100 to 300 nm, we get consistent values of z ranging from 1.43 to 1.6.[35] In passing, we note that one should be cautious about the adverse effect of joule heating when the measurement is to be done in the high-current regime to avoid the finite-size effect. In this regard, while the result reported in Ref. 36 is interesting in that it pioneered *I-V* measurements on high-T_c nanostrips, the extracted critical exponents were likely to be inaccurate because of the difficulty of avoiding Joule heating in nanostrips at high currents. In contrast, we have tested heating in our samples by using the low-frequency technique of Koch *et al.*[37] and we have found that heating does not affect the dc data in samples similar to those measured in this paper at current densities less than $\approx 10^9$ A/m^2.[38]

We are not aware of any way to remove finite-size effects that will allow us to use Eq. (8) to determine ν in films. Instead, we use Eq. (10) which is also applicable to the

vortex-glass transition. By applying a magnetic field we introduce a magnetic length scale $l_B \propto \sqrt{\frac{\Phi_0}{B}}$, which is smaller than the film thickness for $B > 0.1$ T, effectively removing the finite-size limitation in the film. We show $T_c - T_g(H)$ vs H in Fig. 4(b) and find

$$\nu = 0.63 \pm 0.10. \tag{14}$$

It is important to note that there is more disorder in the film than in the crystal. Besides the pointlike oxygen-vacancy disorder as in the untwinned crystals, there are other kinds of disorder existing in the film such as twin boundaries and lattice mismatch caused by the substrate. However, the similar values of z and ν for the untwinned crystal and the film argue that the universality of the phase transition of high-T_c materials is not affected by disorder.

Hence, taking into account results of dc transport measurements on both thin films and thick single crystals, we obtained the critical exponents

$$z = 1.54 \pm 0.14, \tag{15}$$

$$\nu = 0.66 \pm 0.10. \tag{16}$$

III. MICROWAVE MEASUREMENTS ON THIN FILMS

The samples we used for microwave measurements are YBCO films (d=100–300 nm thickness) deposited via pulsed-laser deposition on $NdGaO_3$ and $SrTiO_3$ substrates. ac susceptibility showed T_c of the films around 90 K with transition widths about $\Delta T_c = 0.2$ K. The resistivity of the films is about 120 $\mu\Omega$ cm at 2 K above T_c. Using a Corbino reflection technique, we measured the complex resistivity $\tilde{\rho} = \rho_1 + i\rho_2$ of the samples over a wide frequency range. The measured complex resistivity is converted to conductivity and the mean-field contribution, as determined from the dc resistivity measured from room temperature down to the lowest temperature in the same experiment, is removed.[18,39,40] The process is similar to the method described in[18] to obtain the fluctuation conductivity σ_{fl}.[41]

A. Frequency-dependent fluctuation conductivity and power dependence

According to Fisher-Fisher-Huse (FFH), in zero magnetic field when the current density is small the complex ac fluctuation conductivity should scale as[1]

$$\sigma_{fl}(T,\omega) \approx \xi^{z+2-D} S_{\pm}(\omega\tau). \tag{17}$$

In Eq. (17), ξ is the correlation length and τ is the fluctuation lifetime. The function $S_{\pm}$ is a universal scaling function above (below) T_c, which should be the same for all members of a given universality class. As temperature approaches T_c, both ξ and τ will diverge according to Eqs. (1) and (2).

The scaling functions behave as $S_+(y) \to$ real constant and $S_-(y) \to 1/(-iy)$ for $y \to 0$, reflecting the low-frequency behavior above and below T_c, respectively. As $y \to \infty$, representing $T \to T_c$, $S_+(y) \approx S_-(y) \approx \tilde{c} y^{(D-2)/(z-1)}$ where $\tilde{c}$ is a complex constant and D is the dimensionality of the system.[1,22]

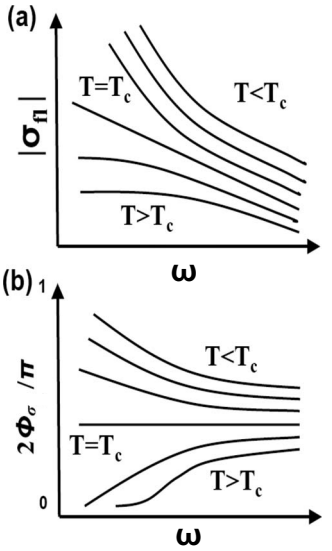

FIG. 6. Schematic plots of (a) Magnitude $|\sigma_{fl}|$ vs ω in log-log scale and (b) phase ϕ_σ vs ω in semilog scale at various temperatures around T_c, based on Fisher-Fisher-Huse ac scaling (Ref. 1).

The complex fluctuation conductivity can be written as $\sigma_{fl} = |\sigma_{fl}| e^{i\phi_\sigma}$ so both the magnitude and phase are predicted to scale

$$|\sigma_{fl}| \approx \xi^{z+2-D} |S_{\pm}(\omega\xi^z)|, \tag{18}$$

$$\phi_\sigma = \Phi_{\pm}(\omega\xi^z). \tag{19}$$

where $\Phi_{\pm}$ is the phase the of the scaling function $S_{\pm}$. At T_c, one expects[22]

$$|\sigma_{fl}| \sim \omega^{-(z+2-D)/z} \tag{20}$$

and

$$\phi_\sigma = \frac{\pi}{2}(z+2-D)/z. \tag{21}$$

Fig. 6 sketches the expected Fisher-Fisher-Huse ac scaling behavior of the magnitude and phase of fluctuation conductivity near T_c.[1,22] Fig. 7 shows the measured complex fluctuation conductivity vs frequency for various temperatures at two different microwave powers. These data display significant and systematic deviations from the expected FFH scaling sketched in Fig. 6. At high frequency, both the magnitude and phase of the fluctuation conductivity look similar to FFH theory. However, as frequency decreases the measured magnitude of the fluctuation conductivity below T_c saturates, instead of bending up. All of the phase isotherms below T_c tend toward zero, indicating ohmic response, instead of approaching $\pi/2$ at low frequency. These deviations are qualitatively similar to the low-current-density deviations of E vs J in dc measurements seen in Fig. 5.[19]

Fig. 7 also shows that the applied microwave power affects the measured fluctuation conductivity, particularly at low frequencies. As frequency decreases, the higher applied microwave power decreases the magnitude of the fluctuation

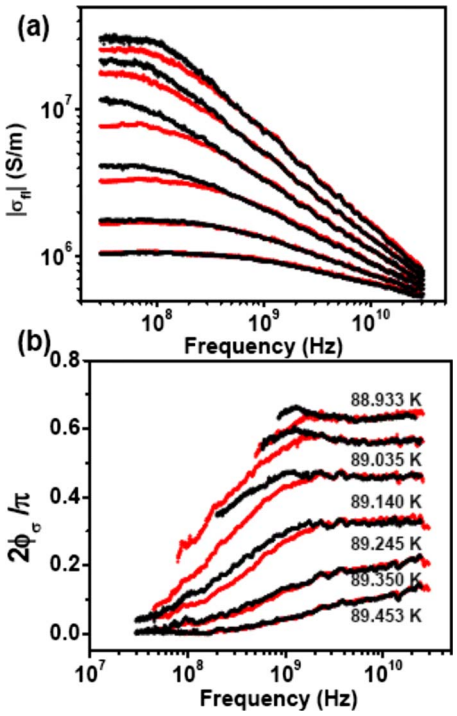

FIG. 7. (Color online) (a) Magnitude $|\sigma_{fl}|$ and (b) phase ϕ_σ vs frequency at various temperatures for a typical YBCO film (xuh139). The black (upper) lines were measured with −22 dBm power while the red (lower) lines were measured with −2 dBm at the same temperature. (For clarity, only every other isotherm is shown.)

conductivity and depresses the phase. These phenomena cannot be explained by the ac scaling equation, Eq. (17), and we need to look at the full version of the FFH dynamic scaling function, which can be written in the following form with assumed dimensionality $D=3$ (Ref. 1)

$$\frac{E}{J} = \xi^{1-z}\chi_{\pm}(J\xi^2, \omega\xi^z, H\xi^2, \ldots). \tag{22}$$

where E is the electric field.

Since the critical point is located in the limit of zero magnetic field H, current density J, and frequency ω, increased applied current should drive the system further away from the transition and thus into the ohmic regime. In our measurement, the magnetic field term $H\xi^2$ can be ignored. The two remaining terms are $J\xi^2$ and $\omega\xi^z$. Qualitatively, at low frequency, $\omega\xi^z$ is small so that the applied power term, $J\xi^2$, has more effect on the fluctuation conductivity.

To illustrate the effect of different powers, $|\sigma_{fl}|$ vs microwave power at different frequencies is plotted in Fig. 8. The power dependence of $|\sigma_{fl}|$ clearly varies with frequency. At low frequencies (60, 80, and 100 MHz), $|\sigma_{fl}|$ vs incident power increases first as power increases (Region I) and then saturates (Region II). At very high power, $|\sigma_{fl}|$ decreases again (Region III). At high frequencies (>0.5 GHz) the fluctuation conductivity is almost power independent.

The important features in Fig. 8 are that large applied power affects the fluctuation conductivity and that even small power depresses the fluctuation conductivity at low

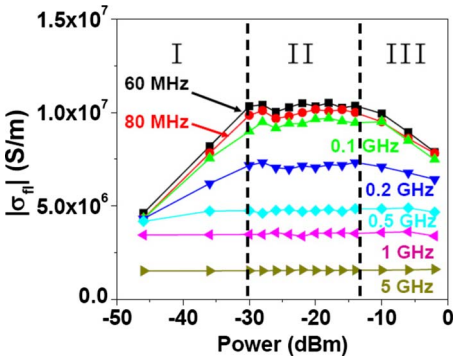

FIG. 8. (Color online) $|\sigma_{fl}|$ vs incident microwave power at different frequencies. ($T=89.140$ K, sample xuh139 below T_c)

frequency. While the high-frequency and high-power data in Fig. 8 are consistent with Eq. (22) and thus can be explained by FFH scaling theory,[1,22,23] the low-power low-frequency behavior is not consistent.

The similarity between this low power and low-frequency deviation and the low-current-density deviation in dc conductivity measurement suggests the presence of a "probed length scale" for a finite frequency. As discussed in connection with Eq. (12) and in the Appendix, when a current with density J is applied, vortex loops (with large r) will "blow out" to infinite size (producing dissipation). Vortex loops with small r shrink and annihilate (with no dissipation). A current-density-induced length scale L_J, given in Eq. (12) separates vortex loops into two categories, depending on their ultimate fate.

The shrinking of a loop takes time. This time depends on the size of the loop, thus relating the size of a vortex loop to a time scale. In ac measurements, small frequency means that large length scales are probed and *vice versa*. By generalizing the order-parameter relaxation-time scale in time-dependent Ginzburg Landau theory[42] one can construct a frequency-dependent length scale

$$L_\omega = \left(\frac{ck_BT_c}{\hbar\omega}\right)^{1/z}\xi(0), \tag{23}$$

where c is a constant of order 1 and $\xi(0)/\xi(T)=|T/T_c-1|^\nu$.

In ac conductivity measurements, the probed length scale should be determined by both frequency and current density. Since the smaller length scale dominates the measured fluctuation conductivity, we propose a plausible expression for the probed length scale for ac measurement $L_{\rm ac}$

$$\frac{1}{L_{\rm ac}} = \frac{1}{L_J} + \frac{1}{L_\omega}. \tag{24}$$

This formula has the correct limits as $J\to 0$ or $\omega\to 0$, which corresponds to frequency-dependent $\omega\xi^z$ scaling or current-density-dependent $J\xi^2$ scaling, respectively. It is also qualitatively consistent with the two-term FFH scaling without the magnetic term $H\xi^2$ of Eq. (22) in the crossover range. Finite-size effects come into play when $L_{\rm ac}$ approaches the thickness of the film.

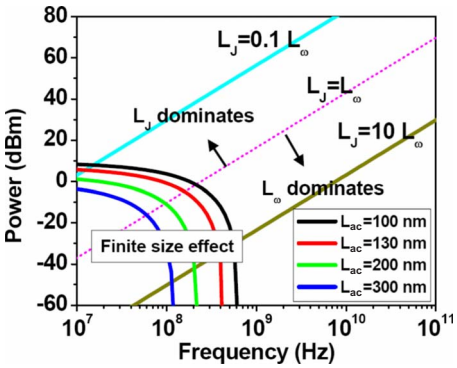

FIG. 9. (Color online) Summary of length scales and finite-size effects in Corbino ac measurements of fluctuation conductivity of YBCO films near T_c. The dotted line in the figure gives the boundary $L_J=L_\omega$. At low frequency and small current density, the probed length scale L_{ac} approaches the thickness of the sample.

Fig. 9 summarizes the length scales in an ac measurement in terms of experimental quantities.[43] In this figure, we use $\xi(0)=5$ Å, $c=1$, and $z=1.5$. The dotted line in the figure gives the boundary $L_J=L_\omega$. To the right and below the dotted line, when $L_\omega \ll L_J$, the frequency-induced length scale dominates, and one observes mainly frequency-dependent scaling of the fluctuation conductivity. Above the dotted line, when $L_\omega \gg L_J$, current-induced nonlinear effects will dominate the behavior. This explains the features shown in Figs. 7 and 8, where the current density has less effect on the fluctuation conductivity at high frequency and a larger effect at low frequency.

At low frequency and small current density, L_{ac} may approach the thickness of the sample (d) or some other length scale that interrupts the fluctuation vortex loops. Hence deviations from the simple scaling theory are expected when $L_{ac} > d$.

In our ac measurements, we want to keep to the limit $L_{ac} < d$ to avoid finite-thickness effect. Hence we choose to stay at low J but high ω. In this region we can find the true critical behavior without getting into any finite-size effect or crossover difficulties. Our previous analysis strayed out of this region and this may account for the larger values of z reported before[18] and elsewhere in the literature.

B. Data-analysis method

In this paper, with very small applied microwave power, −46 dBm (corresponding to $J < 2.2 \times 10^5$ A/m^2), and high-frequency data, we investigated the frequency-dependent fluctuation conductivity around T_c. Conventionally, examining experimental data with the scaling formulas one can search for the temperature at which the conductivity magnitude best fits to a power law and has a constant value of ϕ_σ, to determine T_c and the dynamic critical exponent z. In this analysis process, the determination of T_c is crucial because it directly affects the value of z. Hence we enhanced the temperature stability and conductivity calibration techniques in the experiment, enabling the measurement of high-quality data at small temperature intervals (50 mK).

Using this data, we revised the conventional data-analysis method[18] to determine T_c. One expects a power-law behavior of $|\sigma_{fl}|$ on frequency at T_c, with a change in curvature on either side (a convex function below T_c and a concave function above T_c), as sketched in Fig. 6(a). One also expects a plateau in the conductivity phase vs frequency at T_c with a change in the sign of the slope on either side as sketched Fig. 6(b).

Unlike the dc I-V curve where Strachan *et al.* used an opposite concavity criterion to determine T_c in a dI/dV plot,[29] it is hard to take the frequency derivative of $|\sigma_{fl}(\omega)|$ because of noise. An alternative approach is to do a quadratic fit to the data on a log-log plot. Below T_c, the curve bends up with a positive coefficient of $[\log(\omega)]^2$ and above T_c, the curve bends down with a negative coefficient of $[\log(\omega)]^2$. Hence we did a quadratic fit and found that the coefficient of the $[\log(\omega)]^2$ term changes sign between temperatures 89.192 and 89.245 K, bracketing T_c.

The scaling theory also predicts a constant phase angle $\phi_\sigma(\omega)$ at T_c. $\phi_\sigma(\omega)$ vs $\log \omega$ is known to be a decreasing function below T_c and an increasing function above T_c. A linear fit of $\phi_\sigma(\omega)$ vs $\log f$ also has been done and the result shows its has negative slope at 89.192 K and positive slope at 89.245 K, which is consistent with the quadratic fit result of $\log|\sigma_{fl}(\omega)|$ vs $\log \omega$. The next step is to do a linear fit for $\log|\sigma_{fl}(\omega)|$ verses $\log(\omega)$ to get the slope of $\log|\sigma_{fl}(\omega)|$ and take the average of the $\phi_\sigma(\omega)$ at T_c to obtain the value of z. From this method, we get the critical temperature $T_c = 89.22 \pm 0.05$ K and the critical exponent $z = 1.62 \pm 0.20$.

In addition, we developed another method to determine T_c from the data. Consider the Wickham and Dorsey scaling function above T_c (Ref. 22)

$$S_+(y) = \frac{2z^2\left[1 - \frac{D-2-z}{z} iy - (1-iy)^{(D-2+z)/z}\right]}{y^2(D-2-z)(D-2)}, \quad (25)$$

where $y = \omega\tau \propto \omega\xi^z$. We find at small y, corresponding to temperatures far above T_c, the function $S_+(y)$ is essentially independent of dimensionality D and z because the fluctuation contribution is small. According to Eq. (17), one can write $\sigma_{fl}(T,\omega) = \sigma_0(T)S(\omega/\omega_0)$ where $\sigma_0(T)$ and $\omega_0(T)$ are characteristic conductivity and frequency scales, respectively. Both the phase $\phi_\sigma(\equiv \tan^{-1}[\sigma_2^{fl}/\sigma_1^{fl}])$ of σ_{fl} and the magnitude $|\sigma_{fl}|/\sigma_0$ can be treated as scaled quantities with two temperature-dependent scaling parameters $\omega_0(T)$ and $\sigma_0(T)$. This is a data-collapse method, pioneered by Kitano *et al.*[26] They pointed out that the advantage of this collapse method is the independence of the two scaling parameters $\omega_0(T)$ and $\sigma_0(T)$. In this data-analysis method, the parameters $\omega_0(T)$ and $\sigma_0(T)$ are chosen at each temperature to collapse $\phi_\sigma(T)$ vs ω/ω_0 and $|\sigma_{fl}|/\sigma_0(T)$ vs ω/ω_0 to smooth and continuous curves, without *a priori* determination of T_c or critical exponents.

First $\omega_0(T)$ is determined through a collapse plot of ϕ_σ vs $\omega/\omega_0(T)$ from high temperature to low temperature [see Fig. 10(a)]. Using the feature that $S_+(y)$ is not sensitive to dimensionality D and z far above T_c, the appropriate $\omega_0(T)$ for isotherms far above T_c is chosen to make the measured

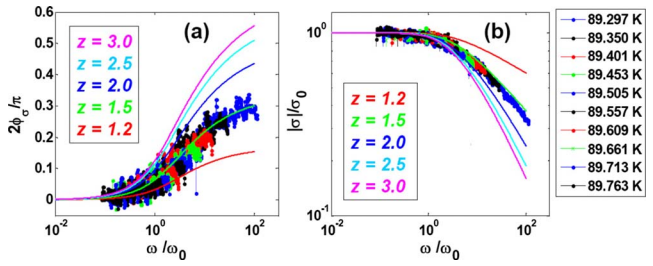

FIG. 10. (Color online) Scaling of phase and magnitude of fluctuation conductivity for sample xuh139 to determine $\omega_0(T)$ and $\sigma_0(T)$. (a) ϕ_σ vs $\omega/\omega_0(T)$; (b) $|\sigma_{fl}|/\sigma_0(T)$ vs $\omega/\omega_0(T)$. Solid lines are the theoretical calculation of $|S_+(y)|$ and $2\phi_{S_+(y)}/\pi$ from Eq. (25) for different values of z, assuming $D=3$. These lines can be used to determine $\omega_0(T)$ and $\sigma_0(T)$ far above T_c. In this figure, only the $\omega_0(T)$ and $\sigma_0(T)$ of the isotherm $T=89.763$ K are shown to make the measured $\phi_\sigma[\omega/\omega_0(T)]$ and $|\sigma_{fl}|/\sigma_0(T)$ vs. $\omega/\omega_0(T)$ overlap with the theoretical prediction. For all the other isotherms, $\omega_0(T)$ and $\sigma_0(T)$ for each temperature are chosen to connect smoothly to the existing curve of $\phi_\sigma[\omega/\omega_0(T)]$ and $|\sigma_{fl}|/\sigma_0(T)$, respectively, to make all the temperature curves collapse into one smooth and continuous curve. The lowest temperature isotherm (blue) appears on the right side of each plot, while the highest temperature isotherm (black) appears on the left.

$\phi_\sigma[\omega/\omega_0(T)]$ overlap with the theoretical prediction from the known scaling function $\phi[S_+(y)]$. Then at temperatures closer to T_c where $S_+(y)$ starts to depend on D and z, $\omega_0(T)$ for each temperature is chosen to connect smoothly to the existing curve of $\phi_\sigma[\omega/\omega_0(T)]$ and to make all the temperature curves collapse into one smooth and continuous curve. This process continues to lower and lower temperature until a temperature is reached where $\phi_\sigma[\omega/\omega_0(T)]$ can not be connected smoothly to the existing curve. In this way, $\omega_0(T)$ for temperature points above T_c can be determined.

To scale the conductivity magnitude, we start with the determined $\omega_0(T)$ for each temperature, then plot $|\sigma_{fl}|/\sigma_0(T)$ vs $\omega/\omega_0(T)$, where $\sigma_0(T)$, similarly to $\omega_0(T)$, is determined for each temperature to make a smooth and continuous curve of $|\sigma_{fl}|/\sigma_0(T)$ vs $\omega/\omega_0(T)$ [see Fig. 10(b)].

Using the power-law assumption for $\omega_0(T)$ and $\sigma_0(T)$, T_c can be determined. Figure 11 shows $\omega_0(T)$ vs t and $\sigma_0(T)$ vs t for different assumed values of T_c. The correct T_c can be determined from the line showing a pure power law. Figure 11(a) shows that the blue line which corresponds to an assumed $T_c=89.25$ K is straightest. Figure 11(b) also shows that the blue line is straightest. From these two figures, T_c is consistently determined to be $T_c=89.25\pm0.05$ K. This result is also consistent with the T_c determined by the revised conventional method.

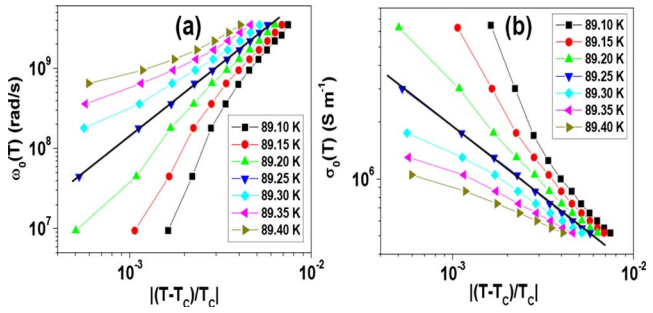

FIG. 11. (Color online) $\omega_0(T)$ vs $|\frac{T-T_c}{T_c}|$ and $\sigma_0(T)$ vs $|\frac{T-T_c}{T_c}|$ for different assumed T_c for sample xuh139 and temperature from 89.297 to 89.763K. The errors of $\omega_0(T)$ and $\sigma_0(T)$ are about the size of the points.

With the value of T_c determined here, we can do a linear fit for $\log|\sigma_{fl}(\omega)|$ verses $\log(\omega)$ to get the slope of $\log|\sigma_{fl}(\omega)|$ and take the average of the $\phi_\sigma(\omega)$ at T_c to obtain the value of z. Through this procedure, we obtained the critical exponent $z=1.55\pm0.20$.

In the procedure outlined above, we take advantage of the broad microwave frequency range of the experiment, which includes frequencies of order $1/\tau$. High quality data at small temperature intervals are essential for the implementation of this method. Another advantage of this method is that many isotherms near T_c contribute to defining the scaling curve, not just the one closest to T_c. This method has the advantage of more precisely determining T_c. So according to the two methods the critical temperature and exponent for sample xuh139 were determined to be $T_c=89.25\pm0.05$ K and $z=1.55\pm0.20$.[40]

The dynamic critical exponent should be sample independent. To check the results, we not only repeated measurements on the same sample but also repeated the experiment on different samples. Films of different thickness ($d=100-300$ nm) were examined, and z was found to be independent of the thickness, keeping in mind the constraints of Fig. 9. Experiments on six samples have been done giving

$$z = 1.55 \pm 0.15. \tag{26}$$

C. ac and dc experiments on the same sample

We also performed dc current-voltage characteristic measurements on the same samples.[40] Typical results are shown in Fig. 12 (with no background subtraction[30]). According to the negative curvature criterion,[29] we determined the critical temperature to be 91.220 ± 0.04 K and the critical exponent $z=1.75\pm0.2$ from the derivative plot in Fig. 12(b). In Fig. 12, all the isotherms tend towards ohmic behavior at low-current density, brought about by $L_J>d$ finite-size effects, as discussed for the data shown previously in Fig. 5.[19] From this data it is clear that when the current density is smaller than 1×10^6 A/m^2, the sample will have only ohmic response around T_c. The −46 dBm applied power in the ac measurement corresponds to a maximum current density of 2.2×10^5 A/m^2($<1\times10^6$ A/m^2). This means that for −46 dBm incident power $L_J>d$, verifying a feature of Fig. 9, and suggesting that one-parameter scaling should work when $L_\omega<L_J,d$. Hence it is appropriate to determine T_c and critical exponents with ac data at −46 dBm applied power.

The difference of T_c between dc and ac measurements is due to the different thermometer positions and temperature-control techniques of the two experimental systems. The resistance vs temperature plots from the ac and dc experiment have a temperature offset about 2.0 K, which is the difference of the determined T_c from these two methods.

In dc measurements, disorder and heating lead one to systematically choose a lower temperature isotherm as T_c, re-

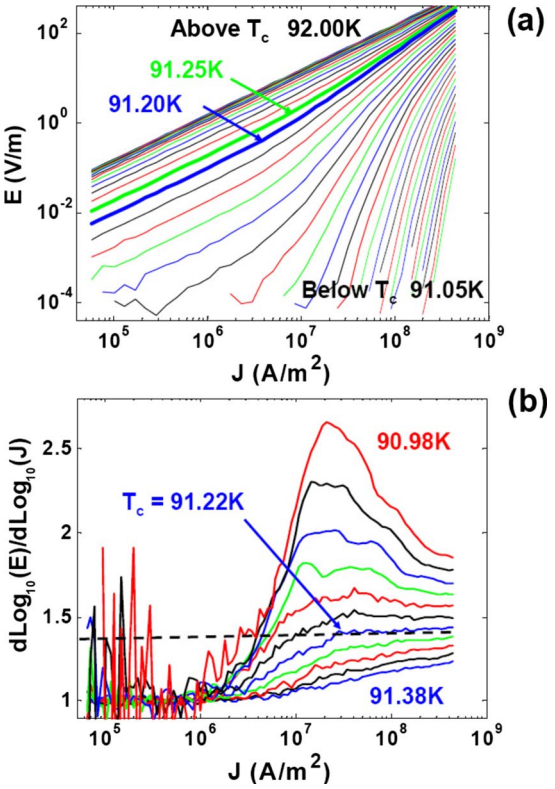

FIG. 12. (Color online) dc current-voltage characteristics measurement, performed after the ac experiment on xuh139 in zero magnetic field. (a) *E-J* isotherms (50 mK apart), (b) $d\log_{10}E/d\log_{10}J$ vs J derivative plot (40 mK apart).

sulting in an enhanced value of z.[30,40] We find that films with lower normal-state resistivity and smaller ΔT_c have smaller values of z.[30] The films used in ac conductivity measurements were grown on $NdGaO_3$ substrates and these films have systematically higher resistivity and larger ΔT_c than films on $SrTiO_3$ substrates. In addition, performing dc measurements on the same film after ac measurements involves more processing steps than a dc measurement alone and may result in additional disorder in the sample. This correspondingly gives larger values of z (Fig. 12). We carefully repeated the dc measurements alone on different YBCO films grown on different substrates ($SrTiO_3$ and $NdGaO_3$) and found that the sample quality does affect the obtained value of z.[40] However, for films with high T_c, sharp transition and small resistivity, the obtained value of $z \approx 1.50$, which is consistent with the ac result $z = 1.55 \pm 0.15$. In addition, dc measurements carried out the same way on high-quality crystals shown in the previous section also gave $z \approx 1.5$.

IV. SUMMARY AND CONCLUSIONS

In this paper, we performed of a variety of complimentary experiments to determine the critical exponents in optimally doped $YBa_2Cu_3O_{7-\delta}$. The dc transport measurements on both thin films and thick single crystals show how finite-thickness effects in the films can confuse interpretation of the data in the limit of small currents. Only with the choice of the proper range of current, can one avoid the finite-thickness effects in films and obtain the correct exponent z, consistent with the value obtained from thick single crystals measurements (where finite-thickness effects are unimportant). We also show how application of a small magnetic field allows the determination of ν in both crystals and films. Using dc transport measurements, we find that the dynamical critical exponent $z = 1.54 \pm 0.14$, and the static critical exponent, $\nu = 0.66 \pm 0.10$ for both films and single crystals.

Microwave measurements on thin films at different frequencies and at different powers have also been performed, which allow us to systematically probe different length scales in the sample. After developing a comprehensive understanding of length scales in microwave measurements, we choose to stay at low J but high ω to find the true critical behavior without getting into any finite-size or crossover effects. dc transport measurements were also performed on the films used in the microwave experiments to provide a further consistency check. These microwave and dc measurements yielded a value of z consistent with the other results, $z = 1.55 \pm 0.15$.

To conclude, using two different measurement methods, we studied the dynamic fluctuation effects of $YBa_2Cu_3O_{7-\delta}$ single crystals and thin films around T_c. The results of both ac and dc measurements agree with the *XY* value for $\nu \approx 0.67$ and with model-*E* dynamics value for $z = 1.55 \pm 0.15$.[3] The neglect of finite-thickness, finite-power, and finite-frequency effects may account for the wide ranges of values for ν and z previously reported in the literature.

ACKNOWLEDGMENTS

The authors thank A. T. Dorsey for insightful discussion. This work has been supported by NSF under Grant No. DMR-0302596 and by the Maryland Center for Nanophysics and Advanced Materials. Y. Ando was supported by KAKENHI under Grants No. 19674002 and No. 20030004, and K. Segawa by KAKENHI under Grant No. 20740196.

APPENDIX: CURRENTS AND LENGTH SCALES IN SUPERCONDUCTORS

In this Appendix we consider a number of length scales in current-carrying superconductors to provide a clearer physical meaning for the length scale L_J of Eq. (12). We first consider a simple model for fluctuations in superconductors, where we assume that the only fluctuations are circular vortex loops (or vortex "smoke rings") of radius r.[34] The energy of such a loop can be written as

$$U_{loop} = 2\pi r \varepsilon(r), \tag{27}$$

where $\varepsilon(r)$ is the energy per unit length of the vortex loop. For a straight vortex

$$\varepsilon(r=\infty) = \frac{1}{4\pi\mu_0}\left(\frac{\Phi_0}{\lambda}\right)^2 K_0\left(\frac{\lambda}{\xi}\right) \approx \frac{1}{4\pi\mu_0}\left(\frac{\Phi_0}{\lambda}\right)^2 \ln\left(\frac{\lambda}{\xi}\right), \tag{28}$$

where K_0 is a modified Bessel function of the second kind and the approximate form holds in the limit of high κ

$\equiv \lambda/\xi$.[44] As a first approximation, we will assume the energy per unit length is constant, given by Eq. (28).

In an infinite superconductor with no applied current, vortex loops of different sizes occur with different probabilities as thermal fluctuations. The probability of finding a loop of size r in a range dr is given by

$$P(r)dr = \frac{e^{-[2\pi\varepsilon(r)/k_BT]r}dr}{\int_{\xi}^{\infty} e^{-[2\pi\varepsilon(r)/k_BT]r}dr}, \tag{29}$$

where interactions between the loops are neglected for simplicity.

We wish to find the size of a typical vortex loop, r_{med}. One way to do this is to find the fraction of loops f with a radius greater than the median radius, or $r > r_{med}$. This fraction will be $f = \frac{1}{2}$, given by

$$f = \frac{\int_{r_{med}}^{\infty} e^{-[2\pi\varepsilon/k_BT]r}dr}{\int_{\xi}^{\infty} e^{-[2\pi\varepsilon/k_BT]r}dr} \equiv \frac{1}{2}. \tag{30}$$

If the energy per unit length of the loop is given by Eq. (28), then Eq. (30) leads to

$$r_{med} = \xi + \frac{k_BT}{2\pi\varepsilon}\ln 2. \tag{31}$$

If the second term on the right-hand side of Eq. (31) dominates, this gives

$$r_{med} \approx \frac{k_BT}{2\pi\varepsilon}\ln 2 \Rightarrow \varepsilon \approx \frac{k_BT}{2\pi r_{med}}\ln 2. \tag{32}$$

Eq. (32) states that, within a factor of ln 2, the total energy of a vortex loop of size r_{med} is equal to k_BT, which is a plausible result.

To check whether the second term on the right side of Eq. (31) is the dominant one, we combine Eqs. (28) and (31). This leads to

$$r_{med} = \xi\left[1 + \frac{\xi}{\left(\frac{\Phi_o^2}{4\pi\mu_0 k_BT}\right)}\frac{\ln 2}{2\pi}\frac{\kappa^2}{\ln\kappa}\right] = \xi\left[1 + \frac{\xi}{\Lambda_T}\frac{\ln 2}{2\pi}\frac{\kappa^2}{\ln\kappa}\right], \tag{33}$$

where Λ_T is defined in Eq. (1.1) of Fisher *et al.*[1] (in cgs units with the Boltzmann constant k_B defined to be 1). The second terms in Eqs. (31) and (33) dominate in the critical regime because ξ diverges while Λ_T is fixed.

For simplicity, we drop the ln 2 in Eq. (31) and use the physically plausible result

$$r_{med} \equiv \frac{k_BT}{2\pi\varepsilon}. \tag{34}$$

Next consider that a current per unit area J is applied in a direction perpendicular to the plane of the loop. The total Lorentz force acting outward on the loop is

$$F_{ext} = 2\pi r J\Phi_0. \tag{35}$$

The energy defined in Eq. (27) gives rise to an inward force that the loop exerts on itself, $-2\pi\varepsilon$. Summing the forces and finding the point where the net force is equal to zero leads to a critical loop size

$$r_o = \frac{\varepsilon}{\Phi_0 J}, \tag{36}$$

where, for simplicity, $\varepsilon(r)$ is again assumed to be independent of r. Note that Eq. (36) is *not* the equation for the current-dependent length scale L_J.

Physically, if a vortex loop has $r > r_o$, the external current blows out the loop to infinite size; this process leads to dissipation. If $r < r_o$, the vortex loop shrinks and annihilates. One can interpret Eq. (36) in a different but equivalent way. The presence of a current density J significantly alters the population of vortex loops with $r > r_o$, and has less effect on the vortex loops with $r < r_o$. In this sense, *a current J* probes the physics on length scales of order r_o and larger. This is the type of language that is sometimes used to describe L_J.

We next discuss the physical significance of comparing the lengths r_o and r_{med}, Eqs. (34) and (36). If $r_{med} \ll r_o$, the current is probing a length scale where there are very few vortex loops. The current thus acts as a very small perturbation on the system. If $r_{med} \gg r_o$, the current is probing a very short length scale, and a large portion of the intrinsic vortex population is being disrupted by the current. The point where $r_{med} = r_o$ thus marks a crossover in the behavior from current acting as a small perturbation to current acting as a large perturbation.

How does a noninfinite film of thickness d affect the physics? It is plausible to say $r_{med} \ll d$ is the three-dimensional limit while $r_{med} \gg d$ is the two-dimensional limit since in the second case most of the vortex loops are interrupted by the film thickness while in the first case they are not. This is true as far as it goes but misses the key point that an applied current probes physics at the scale of r_o and larger. Thus, even in the limit $r_{med} \gg d$, if r_o is small enough, *current will probe physics on length scales smaller than d, and thus the measurement will not be affected by the finite thickness of the film.*

In order for the thickness of the film to have a measurable effect, the current should probe a significant fraction of the loop population and should also probe lengths on the scale of the film thickness. For this to be true, we require

$$r_0 = r_{med} \equiv L_J. \tag{37}$$

Combining Eqs. (34), (36), and (37) gives

$$L_J = \left(\frac{k_BT}{2\pi\Phi_0 J}\right)^{1/2}. \tag{38}$$

This argument leading to Eq. (38) motivates a physical description for L_J: For any J there is a length scale L_J, given by Eq. (38), such that *roughly half the equilibrium (zero current) vortex loop population is strongly affected by J*. This is

the length that one should compare to the film thickness for seeing whether or not measurements are in the two or three-dimensional limit. *The requirements are that there be a significant fraction of the loops that would exceed the film thickness, and, in addition, that the current is probing the same length scale*.

*Also at Joint Quantum Institute, University of Maryland, College Park, MD 20742-4111, USA.

[1] D. S. Fisher, M. P. A. Fisher, and D. A. Huse, Phys. Rev. B **43**, 130 (1991); D. A. Huse, M. P. A. Fisher, and D. S. Fisher, Nature (London) **358**, 553 (1992).

[2] C. J. Lobb, Phys. Rev. B **36**, 3930 (1987).

[3] P. C. Hohenberg and B. I. Halperin, Rev. Mod. Phys. **49**, 435 (1977).

[4] F. S. Nogueira and D. Manske, Phys. Rev. B **72**, 014541 (2005).

[5] J. Lidmar, M. Wallin, C. Wengel, S. M. Girvin, and A. P. Young, Phys. Rev. B **58**, 2827 (1998).

[6] H. Weber and H. J. Jensen, Phys. Rev. Lett. **78**, 2620 (1997).

[7] S. Kamal, D. A. Bonn, N. Goldenfeld, P. J. Hirschfeld, R. Liang, and W. N. Hardy, Phys. Rev. Lett. **73**, 1845 (1994).

[8] S. M. Anlage, J. Mao, J. C. Booth, D. H. Wu, and J. L. Peng, Phys. Rev. B **53**, 2792 (1996).

[9] M. B. Salamon, S. E. Inderhees, J. P. Rice, B. G. Pazol, D. M. Ginsberg, and N. Goldenfeld, Phys. Rev. B **38**, 885 (1988); M. B. Salamon, J. Shi, N. Overend, and M. A. Howson, *ibid.* **47**, 5520 (1993); M. B. Salamon, W. Lee, K. Ghiron, J. Shi, N. Overend, and M. A. Howson, Physica A **200**, 365 (1993).

[10] A. Pomar, A. Diaz, M. V. Ramallo, C. Torron, and J. A. Veira, Physica C **218**, 257 (1993).

[11] R. Liang, D. A. Bonn, and W. N. Hardy, Phys. Rev. Lett. **76**, 835 (1996).

[12] N. Overend, M. A. Howson, and I. D. Lawrie, Phys. Rev. Lett. **72**, 3238 (1994).

[13] V. Pasler, P. Schweiss, C. Meingast, B. Obst, H. Wuhl, A. I. Rykov, and S. Tajima, Phys. Rev. Lett. **81**, 1094 (1998).

[14] S. E. Inderhees, M. B. Salamon, N. Goldenfeld, J. P. Rice, B. G. Pazol, D. M. Ginsberg, J. Z. Liu, and G. W. Crabtree, Phys. Rev. Lett. **60**, 1178 (1988); S. E. Inderhees, M. B. Salamon, J. P. Rice, and D. M. Ginsberg, *ibid.* **66**, 232 (1991).

[15] N. C. Yeh, W. Jiang, D. S. Reed, U. Kriplani, and F. Holtzberg, Phys. Rev. B **47**, 6146 (1993).

[16] J. M. Roberts, Brandon Brown, B. A. Hermann, and J. Tate, Phys. Rev. B **49**, 6890 (1994).

[17] T. Nojima, T. Ishida, and Y. Kuwasawa, Czech. J. Phys. **46**, 1713 (1996).

[18] J. C. Booth, D. H. Wu, S. B. Qadri, E. F. Skelton, M. S. Osofsky, A. Pique, and S. M. Anlage, Phys. Rev. Lett. **77**, 4438 (1996).

[19] M. C. Sullivan, D. R. Strachan, T. Frederiksen, R. A. Ott, M. Lilly, and C. J. Lobb, Phys. Rev. B **69**, 214524 (2004).

[20] K. Moloni, M. Friesen, S. Li, V. Souw, P. Metcalf, L. Hou, and M. McElfresh, Phys. Rev. Lett. **78**, 3173 (1997).

[21] P. Voss-de Haan, G. Jakob, and H. Adrian, Phys. Rev. B **60**, 12443 (1999).

[22] R. A. Wickham and A. T. Dorsey, Phys. Rev. B **61**, 6945 (2000).

[23] D. N. Peligrad, M. Mehring, and A. Dulčić, Phys. Rev. B **69**, 144516 (2004).

[24] G. Nakielski, D. Görlitz, C. Stodte, M. Welters, A. Krämer, and J. Kötzler, Phys. Rev. B **55**, 6077 (1997).

[25] K. D. Osborn, D. J. Van Harlingen, V. Aji, N. Goldenfeld, S. Oh, and J. N. Eckstein, Phys. Rev. B **68**, 144516 (2003).

[26] H. Kitano, T. Ohashi, A. Maeda, and I. Tsukada, Phys. Rev. B **73**, 092504 (2006).

[27] K. Segawa and Y. Ando, Phys. Rev. Lett. **86**, 4907 (2001).

[28] K. Segawa and Y. Ando, Phys. Rev. B **69**, 104521 (2004).

[29] D. R. Strachan, M. C. Sullivan, P. Fournier, S. P. Pai, T. Venkatesan, and C. J. Lobb, Phys. Rev. Lett. **87**, 067007 (2001).

[30] S. Li, Ph. D. thesis, University of Maryland, 2007, http://hdl.handle.net/1903/7276

[31] M. C. Sullivan, T. Frederiksen, J. M. Repaci, D. R. Strachan, R. A. Ott, and C. J. Lobb, Phys. Rev. B **70**, 140503(R) (2004).

[32] The isotherms 93.838 and 93.836 K are not shown in Fig. 2(a) for clarity.

[33] P. J. M. Wöltgens, C. Dekker, R. H. Koch, B. W. Hussey, and A. Gupta, Phys. Rev. B **52**, 4536 (1995).

[34] A. K. Nguyen and A. Sudbo, Phys. Rev. B **60**, 15307 (1999) and references cited there in.

[35] Our previous work (Ref. 45) reported $z \approx 2$. This included a normal-state background subtraction [following W. J. Skocpol and M. Tinkham, Rep. Prog. Phys. **38**, 1049 (1975)].This subtraction is not valid in the critical regime, at or near T_c. Our previous work, when reanalyzed, yields $z \approx 1.5$.

[36] Y. Ando, H. Kubota, and S. Tanaka, Phys. Rev. Lett. **69**, 2851 (1992).

[37] R. H. Koch, V. Foglietti, W. J. Gallagher, G. Koren, A. Gupta, and M. P. A. Fisher, Phys. Rev. Lett. **63**, 1511 (1989).

[38] D. R. Strachan, Ph.D. thesis, University of Maryland, 2002; M. C. Sullivan, Ph.D. thesis, University of Maryland, 2004.

[39] J. C. Booth, D. H. Wu, and S. M. Anlage, Rev. Sci. Instrum. **65**, 2082 (1994).

[40] H. Xu, Ph. D. thesis, University of Maryland, 2007, http://hdl.handle.net/1903/7587

[41] Because the ac mean-field conductivity remains finite and well behaved through T_c, and because the critical regime is wide, a mean-field subtraction can be performed with little effect on the determined critical behavior.

[42] M. Tinkham, *Introduction to Superconductivity* (McGraw-Hill, New York, 1975).

[43] The sample presents a short-circuit termination to the transmission line, to good approximation, resulting in a relation between applied microwave power and current density in the Corbino disk, $J(r) = \sqrt{2P/Z_0}/\pi r t_0$, where Z_0 is the characteristic impedance of the coaxial cable, t_0 is the thickness of the measured sample, and $J(r)$ is the current-density amplitude at the distance r from the center of the Corbino disk. The maximum current density $J_{\max}$ is at the inner radius of the Corbino disk.

[44] T. P. Orlando and K. A. Delin, *Foundations of Applied Superconductivity* (Addison-Wesley, Reading, Massachusetts, 1991), p. 281.

[45] M. C. Sullivan, D. R. Strachan, T. Frederiksen, R. A. Ott, and C. J. Lobb, Phys. Rev. B **72**, 092507 (2005).